J Mater Sci: Mater Electron **(2023) 34:2328**

Al_2O_3/Si NPs multilayered antireflective coating to enhance the photovoltaic performance of solar cells

A. Ramos-Carrazco[1,2], D. Berman-Mendoza[1,2,*], R. Ramirez-Espinoza[1], R. García Gutierrez[1,2], J. L. Vazquez-Arce[3], R. Rangel[4], R. Melendrez-Amavizca[1], and P. Bartolo-Pérez[5]

[1] *Departamento de Investigación en Física, Universidad de Sonora, Blvd. Luis Encinas y Rosales, Z.P. 83000 Hermosillo, Sonora, Mexico*
[2] *Departamento de Física, Universidad de Sonora, Apartado Postal 5-088, Z. P. 83000 Hermosillo, Sonora, Mexico*
[3] *Centro de Investigación Científica y de Educación Superior de Ensenada, C.P. 22860 Ensenada, Baja California, México*
[4] *División de Estudios de posgrado de la Facultad de Ingeniería Química, Universidad Michoacana de San Nicolás de Hidalgo, Gral. Francisco J. Múgica S/N, Ciudad Universitaria, Z.P. 58030 Morelia, Michoacán, Mexico*
[5] *Departamento de Física Aplicada, Cinvestav, Unidad Mérida, Yucatán, Mexico*

Received: 30 August 2023
Accepted: 18 November 2023
Published online: 16 December 2023

ABSTRACT

In the present work, the enhancement in the efficiency of commercial solar cells through the use of Al_2O_3/ SiNPs multilayer antireflecting coating, is reported. The Al_2O_3 coatings were deposited by the atomic layer deposition technique, while the silicon nanoparticles were synthesized using a water-dispersible methodology. Based on photoluminescence and absorbance studies of the SiNPs, the underlying mechanism for this improvement can be attributed to the luminescent down-shifting effect. Thermoluminescence studies were achieved to confirm the formation of the Al_2O_3 layer. The thickness of the Al_2O_3 thin films were determined by spectroscopic ellipsometry in a range of 25 to 30 nm, while a SiNPs size of approximately 3 nm was obtained using dynamic light scattering method. The coatings of Al_2O_3 with SiNPs nanoparticles were deposited over solar cells to study their efficiency enhancement. Under a simulated one-sun illumination, coated solar cells achieved an enhancement of 6.74 mA/cm^2, in short-circuit current density; while a 54.9% in power conversion efficiency increase was achieved, relative to those obtained for a pristine cell. The results show that the efficiency of solar cells can be significantly increased by combining the downshifting effect of the Si nanoparticles and the antireflective properties of the Al_2O_3 films.

Address correspondence to E-mail: dainet.berman@unison.mx

https://doi.org/10.1007/s10854-023-11667-1

1 Introduction

An important research trend, at the fore front of world´s attention is the improvement and better use of solar energy, through the use of solar cells (SC), carried out through the photovoltaic effect [1–3]. Usually, SC are manufactured using silicon as active material due to their abundance, technological development, electrical characteristics, and adequate efficiency for power conversion [4–6]. In recent years, a great effort has been made by various research groups to improve the energy conversion efficiency of photovoltaic devices through different methods that include surface nano-texturization, anti-reflective coatings, and surface passivation schemes, among others. However, refraction and reflection have been detected as main factors involved in decrease in the efficiency of solar cells [7–10]. Consequently, several coating materials have been focused to solve these major challenges. Particularly, the power loss on silicon-based devices due to reflections at the material interfaces, is still on discussion [11].

Since pure silicon cell reflects 31–51% of the light reaching their surface, it would only transmit in about 70% of IR and 50% of UV of the sunlight to the cell [12]. Because of that, it is evident that an improvement in the efficiency of silicon solar cells is necessary [13–15]. On that sense, antireflecting coatings (ARC) have been incorporated in the solar cell fabrication process [16–18]. Commonly, ARCs are applied on the cover glass and/or directly on the SC and recently; these coatings have been combined with other materials to also consider the soiling problem, using self-cleaning process [19]. SiO_2, MgF_2, SnO_2, SiC, TiO_2, Al_2O_3, and ZrO_2 are the materials most commonly used as antireflection coating in photovoltaic solar cells [20]. In applications where, in addition to antireflective coatings, self-cleaning is required, Al_2O_3 is one of the most suitable materials; when this material is applied in double and triple layer coatings, satisfactory results are obtained in terms of adhesion to the surface and durability. In multilayer anti-reflective coatings, the use of Al_2O_3 reduces reflectance because it is a material with a low refractive index, which increases light transmittance [19]. Different fabrication methods have been employed for ARC production such as magnetron sputtering [21], e-beam evaporation [22], chemical vapor deposition (CVD) [23], pulsed laser deposition (PLD) [24], dip coating [25] and sol–gel, among others [26, 27]. It has been found that the ALD-grown Al_2O_3 coating has an average transmittance of 99% in the range of 350 nm to 800 nm and this method of preparation ARC has the advantage of broadband antireflection performance, is a simple fabrication process, and can be obtained using a batch processing [28].

Another problem, currently related to solar cells fabrication, is that these devices do not get to take full advantage of the UV solar radiation. That is the underlaying reason that motivates an intense search for alternatives and, for better use of this high energy radiation. Those materials which make use of this segment of the electromagnetic spectrum, do it through an effect known as down shifting effect. This phenomenon consists of the absorption of high-energy photons with their subsequent re-emission with a lower energy, towards the depletion region of the solar cell. In this way, these photons will contribute to the photocurrent increase [29, 30].

Different materials have been explored to enhance the power conversion efficiency through the down shifting phenomena of solar cells using nanoparticles (NPs), and its behavior can be approached to a conductor or semiconductor. Considering the first one, a promising method was reported incorporating localized surface plasmon resonance produced by Au, Ag and Cu nanoparticles [31–33]. The application of metallic NP_S in photovoltaics has been widely studied because they can be simply deposited without modifying the device structure; thus, significantly increasing the efficiency of commercial solar cells [34].

From another perspective, semiconductor NPs represents a promising and cost-effective alternative to improve the efficiency of photovoltaic devices. The down shifting phenomena produced by silicon nanoparticles (SiNPs), has been reported to increase the efficiency of the solar cells [35]. In this process, luminescent nanoparticles absorb a high energy photon, which, in turn, emit photons at longer wavelengths. A recent result of our research group using a down shifting conversion process, has shown an increase in a range of 11 to 17% in the solar cells efficiency, has been obtained [36, 37].

In this work it is presented a combined structure consisting of a Al_2O_3/ SiNPs multilayer antireflective coating. The SiNPs presented a 459 nm emission in the visible range, revealed by photoluminescent spectroscopy. The Al_2O_3 thin films deposited by atomic layer deposition (ALD) containing silicon NPs, described a combined effect, acting as antireflective coating and showing the down shifting effect, which resulted in an increase in the solar cell efficiency. The Al_2O_3/SiNPs multilayer coating was deposited over commercial Silicon solar cells, improving their efficiency up to 54%.

2 Experimental procedure

2.1 Fabrication

2.1.1 *Nanoparticles synthesis*

For the present study, the silicon nanoparticles were prepared by adding 1 mL of APTES to 4 mL of deionized water (DI-water) and stirring it for 10 min. After that, 1.25 mL of 0.1 M sodium L-ascorbate ≥ 98% ($C_6H_7NaO_6$) (SA) was added to the previous mixture and stirred by 20 min, as is shown in Fig. 1. The SiNPs were deposited over solar cells by means of the spin-coating methodology, which consists of depositing a film from a solution, on a SC substrate placed on a rotating system. The solution was spin coated over the surface, creating a uniform layer. In this way, 1 mL of the SiNPs solution was deposited on the SC, at a speed of 4000 RPM for 60 s. To study the method reproducibility, four samples labeled as A1-A4 were synthesized under the same parameters.

2.1.2 *Al_2O_3 deposited by ALD*

To synthesize the Al_2O_3 thin films, trimethyl-aluminum (TMA) (98%, purity) was used as precursor, H_2O as reactant material, an oxygen source, and N_2, (99.999%, purity) as a purging gas, with a volumetric flow of 100 sccm, at 180 °C. The method consists of repetitive deposition cycles occurring inside the reaction chamber, alternating the precursor gas, the reactant gas intake, as well as, the nitrogen flow, used as purging gas. That procedure is summarized in Table 1.

2.1.3 *Al_2O_3 with silicon nanoparticle, deposited over solar cells*

The SiNPs working conditions previously mentioned were used, as well as those described for the Al_2O_3 thin films fabrication. Figure 2 shows a scheme of the

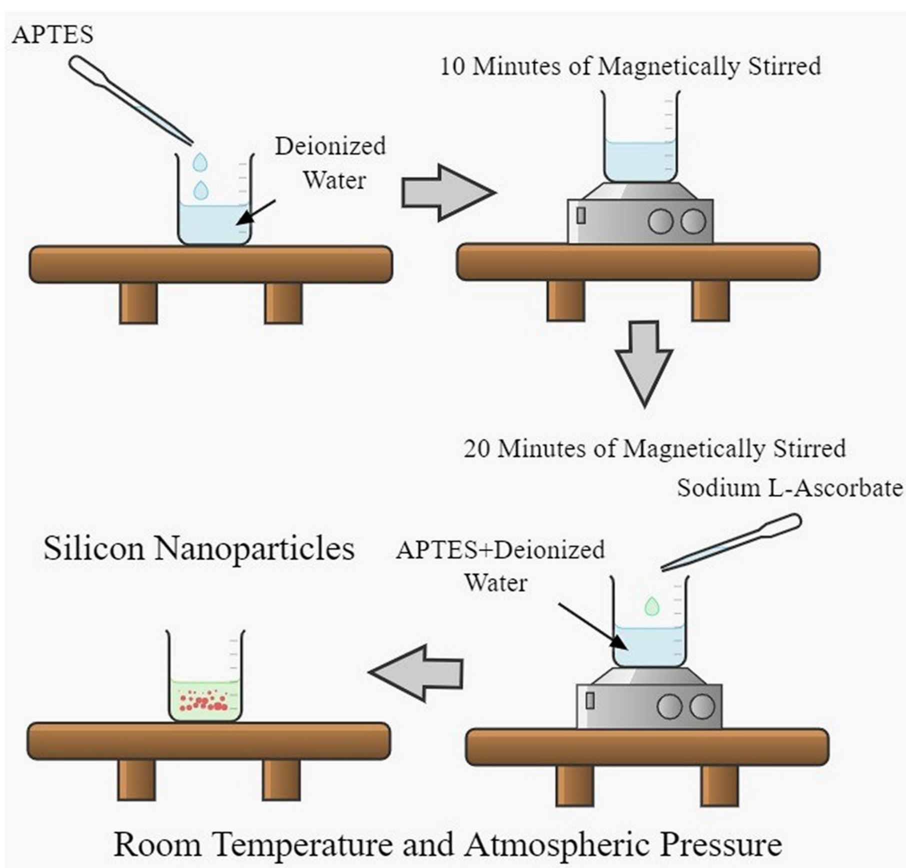

Fig. 1 Schematic diagram of the procedure to synthesize silicon nanoparticles

Table 1 Parameters of Al_2O_3 nanolaminates deposited by ALD

Parameter	Value
Cycles	100
Temperature	~ 180 °C
Time of TMA	20–125 ms
TMA time of purge	15 s
Time of H_2O	100 ms
H_2O time of purge	15 s
Work pressure	1.8 Torr
Nitrogen flux	~ 101 sccm

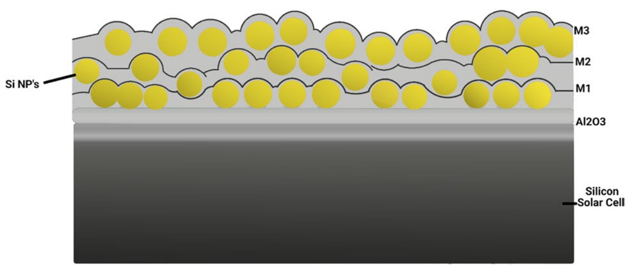

Fig. 2 Al_2O_3 thin films with silicon nanoparticles deposited over solar cell

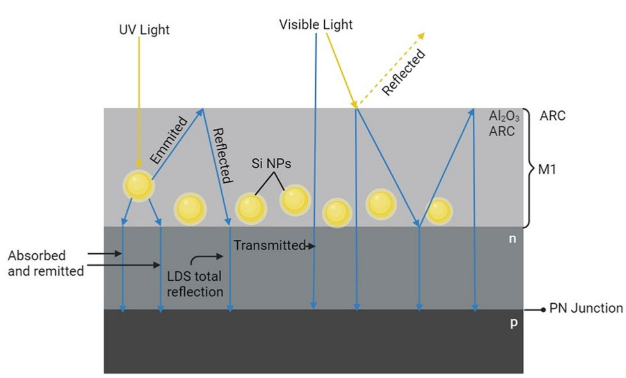

Fig. 3 Schematic diagram showing the mechanism of photon trajectories in the coating of Al_2O_3 and SiNPs

structure produced after achieving a three-layer coating of Al_2O_3 with silicon nanoparticles. The electrical measurements were carried out after depositing each layer represented in Fig. 2 as M1, M2 and M3.

Figure 3 shows the interaction between the incident radiation and the Al_2O_3-SiNPs ARC. The UV region of the incident solar spectrum will be absorbed by the embedded silicon nanoparticles and reemitted as visible light. Due to the refractive index of the ARC, an important part of the isotropic emission of the SiNPs

Table 2 Average size and standard deviation of SiNPs

Sample	Average (nm)	SD (nm)
A1	3.49	0.91
A2	3.59	0.80
A3	3.46	0.63
A4	2.96	0.33

will be reflected from the ARC-air interface and transmitted to the solar cell surface. The wavelength region within visible range, where silicon solar cells had good spectral response, will be efficiently transmitted to the device due to the antireflective effect of the Al_2O_3 thin film. The synergistic effect of the down-shifting properties of the SiNPs and the antireflective effect of the Al_2O_3 thin film maximizes the electron–hole pair generation within the PN junction which is reflected as enhanced power conversion efficiency on the solar cell.

3 Results and discussions

3.1 SiNPs characterization

The size distribution of SiQDs was measured with a Malvern Zetasizer Nano Series using dynamic light scattering method (DLS). The A1–A3 samples have an average size of 3.50 nm with a standard deviation of 0.91 nm. By contrast, the A4 sample shows an average size of 2.99 nm with a standard deviation of 0.33 nm, as can be seen in Table 2. Those results demonstrate that silicon nanoparticles have a very controlled size and distribution. Because all the samples presented a similar size distribution as exhibited in Fig. 4a, the sample A3 was selected for optical analyzes. This sample presented an absorption spectrum tapering off beyond ~ 500 nm as is shown in Fig. 4b. Employing the Tauc´s Law, from the absorption spectrum, it is possible to determine the bandgap energy value of the SiNPs. Accordingly, to a direct bandgap material:

$$hv = A(\alpha hv)^{1/n} + E_g \tag{1}$$

where α is the absorption coefficient, h is the Planck´s constant, v is the photon frequency, E_g is the bandgap, A is a constant and $n = 1/2$ given the nature of the electronic transitions (direct allowed). Figure 4c shows the $(\alpha hv)^2$ vs hv graph, as well as the linear fitting, and the obtained E_g value. The average E_g determined from

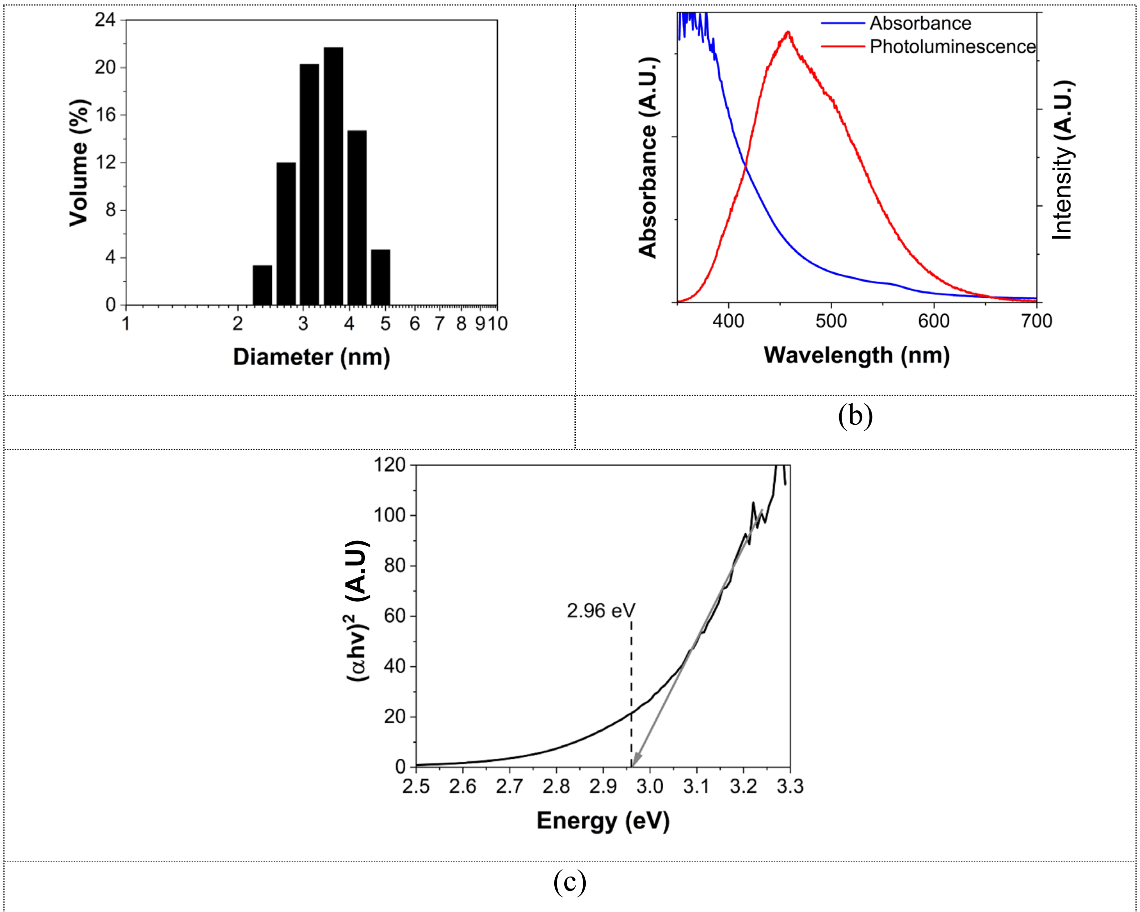

Fig. 4 Histogram showing the size distribution of silicon nanoparticles, **b** absorption and Photoluminescence spectra of SiNPs, **c** band-gap determination of SiNPs

the samples, was 2.96 ± 0.03 eV. The absorbance and E_g results demonstrate the efficiency of the synthesis method. Figure 4b shows the photoluminescence response of the A3 SiNPs sample. The synthesized silicon nanoparticles were measured with a 325 nm Kimmon IK Series He-Cd laser, an Ocean Optics model Red Tide USB650 detector, provided with an Ocean Optics View Spectroscopy Software version 1.6.7. The PL spectra consists of broadband signal extending from 375 to 650 nm in all cases with a peak position at 459 nm.

The nanoparticles obtained in this stage were subsequently deposited on commercial solar cells without coating. It was also used to develop the coatings by combining them with Al_2O_3 thin films that were also deposited on commercial solar cells, achieving a substantial increase in their efficiency.

3.2 Characterization of Al_2O_3

3.2.1 *Thermoluminescence of Al_2O_3*

Thermoluminescence (TL) experiments were carried out using the RISØ TL/OSL reader model TL DA-20 equipped with a $^{90}Sr/^{90}Y$ beta particle source with an activity of 40 mCi and a dose rate of 5 Gy/min, with a linear heating rate of 5 °C/s from room temperature up to 300 °C in a N_2 atmosphere.

Figure 5 shows the behavior of the thermoluminescence of the Al_2O_3 thin film deposited with 300 ALD cycles, it was exposed to beta radiation in a dose range of 83 to 7200 Gy. The TL glow curves are displayed at different doses, indicating that as the radiation dose increases, the thermoluminescence signal is also increased. A broad TL band is observed in the range

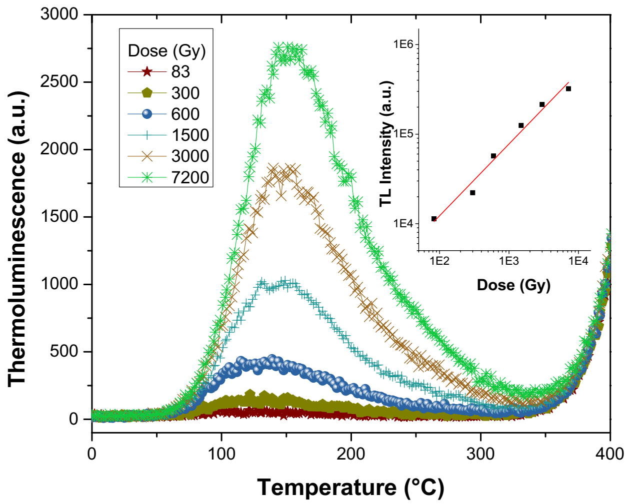

Fig. 5 Glow curve of thermoluminescence spectrum of Al_20_3

from 50 to 350 °C, apparently composed of several thermoluminescence peaks, with a maximum around 150 °C. In the inset of Fig. 4, can be appreciate the area under the curve of the TL with respect to radiation doses, a well-defined linear behavior without apparent saturation is observed. The TL results are very close to those reported in the literature for Al_2O_3 [38–40].

3.2.2 *X-ray photoelectron spectroscopy of Al_2O_3*

The X-ray photoelectron spectroscopy (XPS) survey spectra (0–1250 eV) of Al_2O_3 thin films are shown in Fig. 6. XPS was performed with a Perkin Elmer PHI5100 to study the chemical composition on the different samples; the studies were done with a Mg source at 15 keV and 300 W with a pressure of 4×10^{-8} Torr. The observed signals are associated to Al and O, meaning that the films are free of contaminants. It can be noticed the existence of C1s peaks, which is usually found as residual trace and it is considered as the calibration reference [41–43].

Figure 7 shows (a) the peak corresponding to aluminum 2p (74.9 eV) and (b) O 1s (531.22 eV), which match well when compared to the corresponding data reported in the literature considering the Al_2O_3 compound.

3.2.3 *Spectroscopic ellipsometry determinations.*

As detailed in the experimental part, three layers of 20 nm Al_2O_3 were stacked with three layers of SiNP's. Figure 8a, b shows the raw ellipsometry Psi (Ψ) and delta (Δ) of the stacked three layers, i.e., 20, 40, and 60 nm. The ellipsometry data was taken at an angle of 65°. Two points from the raw measurements can be highlighted. As the thickness increases, the interference shifts to longer wavelengths, and the delta (Δ) is more sensitive to thickness change than psi (Ψ). Both assertions agree with the basic theory of ellipsometry [44].

On the other hand, Fig. 8a and b also shows the fitting used with the Cauchy model to process the data. Cauchy's theory is usually used in ellipsometry measurements of transparent oxides with high bandgaps, such as Al_2O_3 [45]. Its basic formula for the refractive index calculation is as follows:

$$n(\lambda) = A + \frac{B}{\lambda^2} + \frac{C}{\lambda^4} \quad (2)$$

where A, B, and C are the Cauchy parameters. Figure 8c shows the refractive index profile of the three Al_2O_3 thicknesses calculated with the Cauchy model. In addition, the refractive index of bulk Al_2O_3 taken from the T. Winchester handbook was added, for comparison purposes [46].

In Fig. 8d, we compare the refractive index of the Al_2O_3 films vs thickness, where we add more points for better visualization. As the thickness of Al_2O_3 increases, the refractive index increases. Firstly, the abrupt change in the refractive index, around 10 nm, is due to the growth mode of islands and layers, which predominate in the ALD process during the initial growth cycles [47, 48]. The film is not entirely homogeneous during the first layers, so the refractive index is low.

The other point to highlight is the difference in the refractive index in comparison to bulk Al_2O_3 [46]. This, is mainly due to the density of the Al_2O_3. Bulk Al_2O_3 crystals are usually fabricated at high temperatures, producing high-density materials.

3.3 SEM characterization of Al_2O_3 thin films with SiNPs

Figure 9 shows the SEM images of the Al_2O_3 and SiNPs over solar cells. The morphology was studied

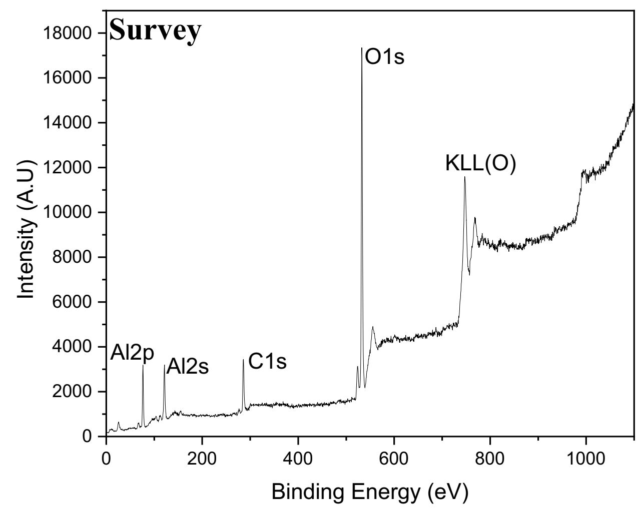

Fig. 6 XPS survey spectra of Al_2O_3 nanolaminates

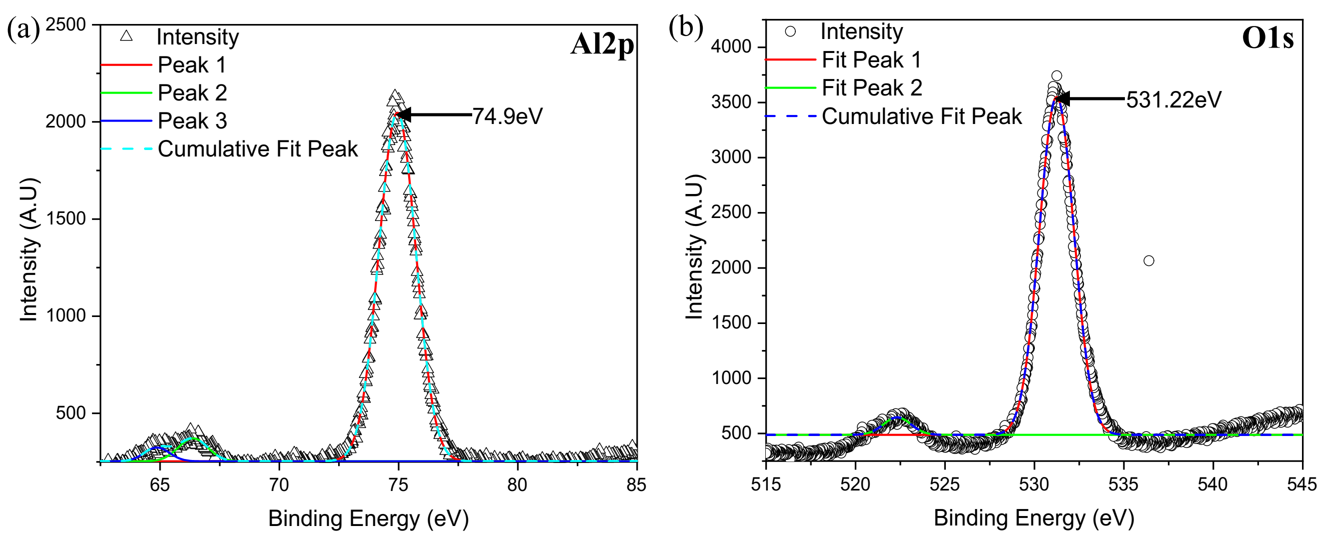

Fig. 7 Spectra showing the main XPS peaks of **a** Al 2p and **b** O 1s

with a JSM-7600F JEOL FESEM microscope, at the working conditions of 20 keV and 10^{-6} Torr. Figure 9a shows the cross-section image of the solar cell with the Al_2O_3 coating with SiNPs, in this image the coating is on the left side. Figure 9b shows the image of surface cell that contains the aluminum contact and the coating of Al_2O_3 with SiNPs, as illustrated in the red rectangle. It is also observed that the coating is conformal because it follows the shape of the surface on which it was deposited. Figure 9c shows the high magnification SEM image of the Al_2O_3 with SiNPs coating, consisting of 3 layers of 22 nm as proposed in Fig. 1 as M1, M2 and M3.

3.4 Electrical characterization of nanolaminates of Al_2O_3 and silicon nanoparticles

In order to compare the performance of the Al_2O_3/SiNPs multilayer antireflection coating, SiNPs were deposited on solar cells and the *I*–*V* curves were measured as reference. In a first stage, three silicon solar cells were coated with silicon nanoparticles according to the procedure described above, using commercial polycrystalline silicon solar cells (1.9 × 3.9 cm) as substrate. Current–voltage parameters were measured before and after the deposit of the SiNPs using a Keithley model 2400 source meter and the efficiency of the solar cells was determined using an Oriel LCS-100

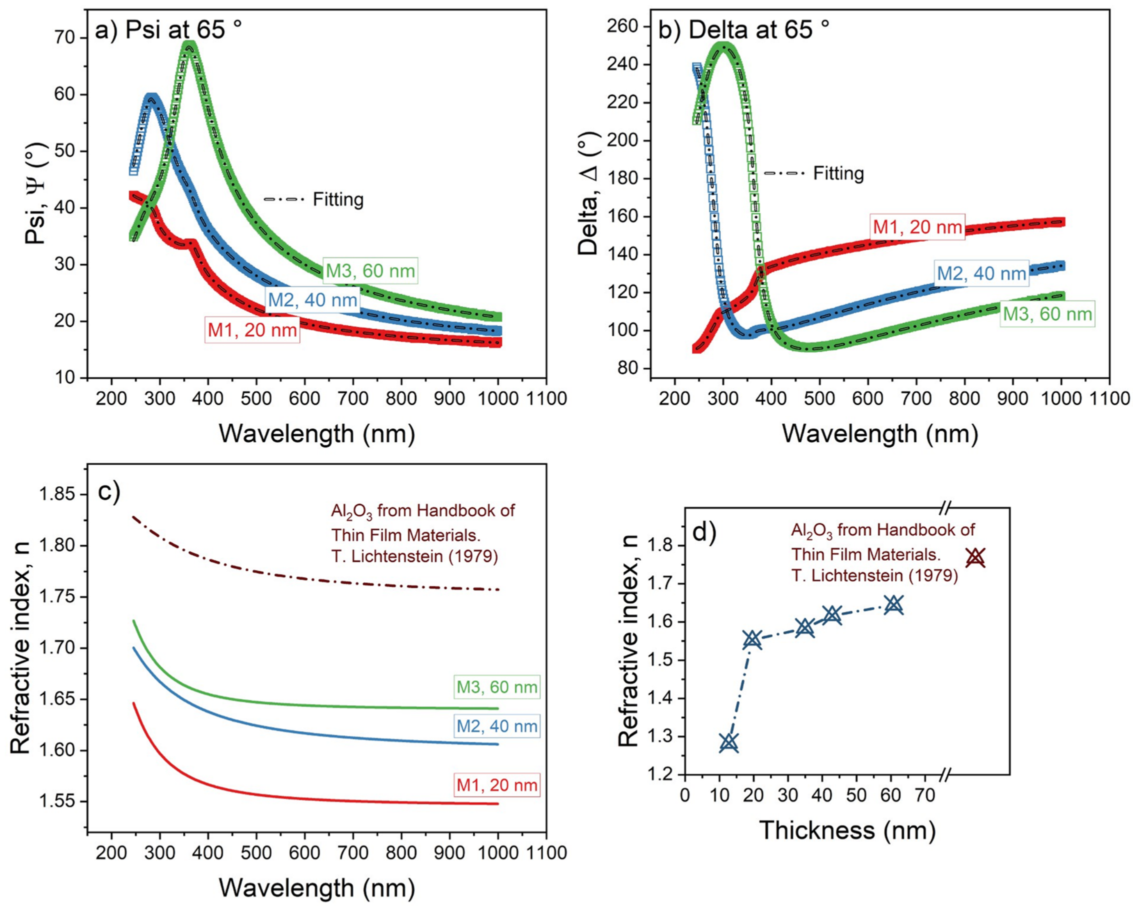

Fig. 8 **a** and **b** Shows the raw ellipsometry Psi (Ψ) and delta (Δ) measured from the three Al_2O_3 layers stacked with SNPs layers. **c** Shows the refractive index vs wavelength of the Al_2O_3, and **d** shows the refractive index vs thickness of Al_2O_3

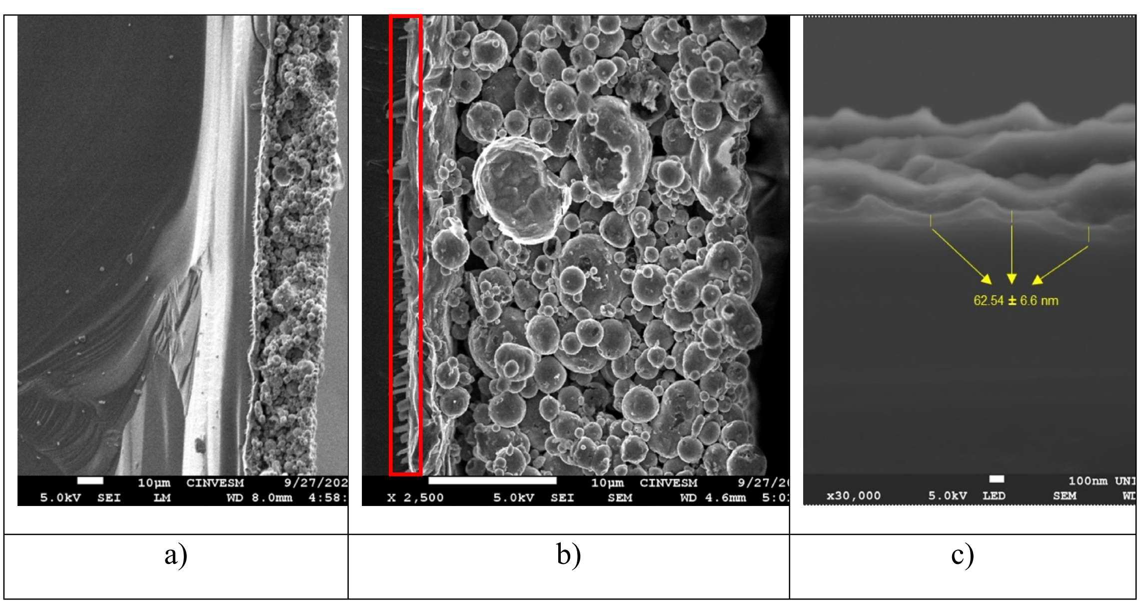

Fig. 9 **a** SEM cross-section image of the solar cell with the Al_2O_3 coating with SiNPs, **b** image of surface cell that contains the aluminum contact and the coating of Al_2O_3 with SiNPs, **c** SEM image of the Al_2O_3 with SiNPs coating

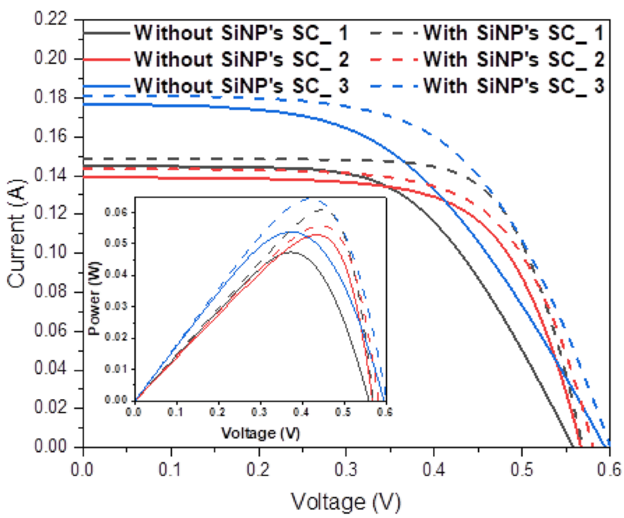

Fig. 10 *I–V* and *P–V* curves of SiNPs over Silicon solar cells

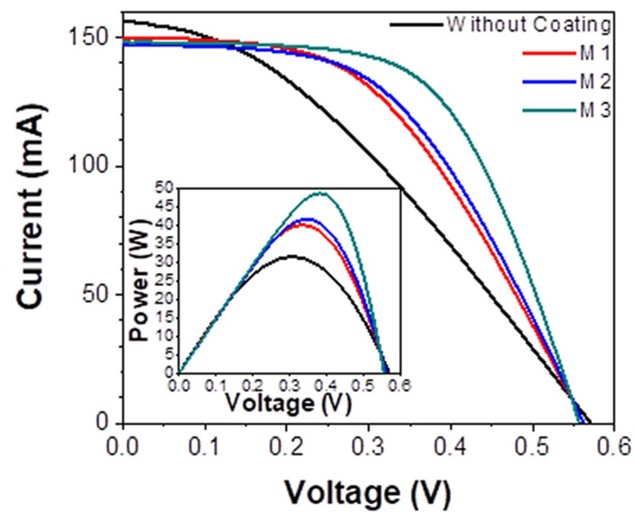

Fig. 11 *I–V* and *P–V* curves of Silicon solar cell (SC_E) covered with Al_2O_3 thin films and SiNPs

solar simulator. Figure 10 shows the results of the electrical characterization and Table 5 shows the open circuit voltage (V_{oc}) and the short circuit current (I_{sc}), which are used to calculate the fill factor of solar cells (FF), being the most important parameter to determine the efficiency of SC.

The results obtained show that the solar cells coated with silicon nanoparticles, increased their efficiency from 6.38 to 8.20% (SC1 + SiNPs), from 7.14% to 7.53% (SC2 + SiNPs), and from 7.26 to 8.68% (SC3 + SiNPs). An increase average of 1.21% and 17.6% was obtained for efficiency and relative efficiency, respectively. The increase in the relative efficiency of solar cells is consistent with the results obtained in previous studies [36].

In a second stage, In Fig. 11, it can be seen that the efficiency of the solar cell increases as the coating cycles composed of Al_2O_3 thin films and silicon nanoparticles, are increased. The pristine solar cell has an efficiency of 4.25% (SC). After performing one coating, it shows an efficiency of 5.42% (SCM1), which increases up to 5.63%, for two coating cycles (SCM2). Finally, after three deposition cycles, it shows an efficiency value of 6.59% (SCM3). The solar cell having three coatings including the encapsulated nanoparticles labeled as SCM3, has a relative efficiency of 54%, as can be shown in Table 6.

In summary, commercial solar cells with an efficiency between 6 and 7% were used, then SiNPs were deposited on these SCs, obtaining efficiencies around 8% on average, as shown in Fig. 9, which yields an increase of 12% in the efficiency of the commercial solar cell. After this, the coatings composed of the antireflective film and SiNPs were deposited. The commercial solar cells with one coating had an efficiency increase of 27%, with two coatings 32% and with three coatings 55%. These results demonstrate that the combined effects of Al_2O_3 ARC and SiNPs improve the efficiency of commercial solar cells outstandingly.

Table 5 Electrical characteristics of Solar cells covered with SiNPs

Sample	$I_{sc}(A)$	$V_{oc}(V)$	$I_{max}(A)$	$V_{max}(V)$	$P_{max}(W)$	η(%)	FF (%)
SC1	0.1449	0.56	0.1279	0.37	0.0473	6.3884	58.34
SC1 + SiNPs	0.1488	0.57	0.1351	0.45	0.0608	8.2038	71.68
SC2	0.1391	0.57	0.1230	0.43	0.0529	7.14	66.73
SC2 + SiNPs	0.1435	0.59	0.1268	0.44	0.558	7.53	65.93
SC3	0.1767	0.6	0.1454	0.37	0.0538	7.2607	50.76
SC3 + SiNPs	0.1812	0.61	0.1533	0.42	8.6896	8.6896	58.26

Table 6 Electrical characteristics of Solar cells covered with thin films of Al_2O_3 and silicon nanoparticles

Solar cells	P_{Max}[W]	η[%]	FF[%]	η_{rel}[%]
SC	0.0315	4.25	34.69	-
SCM1	0.0402	5.42	46.94	27.47
SCM2	0.0418	5.64	49.76	32.55
SCM3	0.0488	6.59	58.82	54.99

4 Conclusions

In the present work, the study of the influence of coatings, based on Al_2O_3 thin films and SiNPs and their effect on increase of the efficiency values of commercial solar cells is presented. The SiNPs were synthetized using a water-dispersible method, while the Al_2O_3 coatings were fabricated by the ALD technique. The SiNPs presented the down shifting effect as was demonstrated by their photoluminescence results. Experimental results showed that the incorporation of silicon quantum dots (Si-QDs) as down-shifting material on the window side of a solar cell, improves the photocurrent generation. That was observed in our samples with a current density increase from 33.42 to 38.28 mA/cm^2 and an open circuit voltage value from 532.57 to 536.20 mV. The coating SiNPs with Al_2O_3 presented a combined effect, behaving as antireflective coating and down shifting material, increasing the solar cell efficiency. The coating of NPs in Al_2O_3 thin films improved their efficiency up to 54.99%. The increase on the efficiency obtained is outstanding with respect to those reported in other works that use only nanoparticles or only antireflective coatings. Therefore, the structure of multilayered antireflective films containing nanoparticles, proposed in this work, opens the possibility of carrying out a more exhaustive investigation on this subject.

Author contributions

All authors contributed to the study conception and design. Material preparation, data collection and analysis were performed by DBM, RRS, ARC, RGG and RMA. JLVA and PBP optically characterized the coating. The first draft of the manuscript was written by DBM, RRS, AR and all authors commented on previous versions of the manuscript. All authors read and approved the final manuscript.

Funding

The authors declare they have no financial interests.

Data availability

All authors declare that all data and materials used in this article comply with the standards in the area of semiconductor devices.

Code availability

Not applied.

Declarations

Conflict of interest The authors have no relevant financial or non-financial interests to disclose.

Ethical approval All authors accepted that the principles of ethical and professional conduct have been followed.

Consent to participate All authors consent to participate in the article.

Consent for publication All authors give their consent for the publication of the article.

References

1. S.R. Wenham, M.A. Green, Silicon solar cells. Prog. Photovoltaic Res. Appl. **4**, 3–33 (1996)
2. L. Fraas, L. Partain, Solar cells and their applications (2nd Edn, Wiley Series in Microwave and Optical Engineering, 2010) ISBN 978–0–470–44633–1
3. A. Blakers, N. Zin, K.R. McIntosh, K. Fong, High efficiency silicon solar cells. Energy Procedia **33**, 1–10 (2013)
4. S.Q. Hussain, S. Kim, S. Ahn, H. Park, A.H.T. Le, S. Lee, RF magnetron sputtered ITO: Zr thin films for the high

efficiency a-Si: H/c-Si heterojunction solar cells. Met. Mater. Int. **20**(3), 565–569 (2014)
5. M. Taguchi, A. Yano, S. Tohoda, K. Matsuyama, Y. Nakamura, T. Nishiwaki, 24.7% record efficiency HIT solar cell on thin silicon wafer. IEEE J. Photovoltaics **4**(1), 96–99 (2014)
6. T. Mishima, M. Taguchi, H. Sakata, E. Maruyama, Development status of high-efficiency HIT solar cells. Sol. Energy Mater. Sol. Cells **95**(1), 8–21 (2011)
7. A.S. Sarkin, N. Ekren, S. Saglam, A review of anti-reflection and self-cleaning Coatings on photovoltaic panels. Sol. Energy **199**, 63–73 (2019)
8. Q. Luo, X. Deng, C. Zhang, M. Yu, C. Zhang, X. Zhou, Z. Wang, X. Chen, S. Huang, Enhancing photovoltaic performance of perovskite solar cells with silica nanosphere antireflection coatings. Sol. Energy **169**, 128–135 (2018)
9. M. Qiang, Z. Wei-Jia, M. Deng-Hao, F. Zhi-Qiang, J. Zhaoyi, Optimal design of quadruple-layer antireflection coating structure for conversion efficiency enhancement in crystalline silicon solar cells. Optik **177**, 123–130 (2019)
10. M. Aleem-Zahid, M. Quddamah-Khokhar, Z. Cui, H. Park, J. Yi, Improved optical and electrical properties for heterojunction solar cell using $Al2O_3$/ITO double-layer anti-reflective coating. Results Phys. **28**, 104640 (2021)
11. G. Velu-Kaliyannan, S. Velmurugan-Palanisamy, R. Rathanasamy, M. Palanisamy, S. Kumar-Palaniappan, M. Chinnasamy, Influence of ultrathin Gahnite anti-reflection coating on the power conversion efficiency of polycrystalline silicon solar cell. J. Mater. Sci. **31**, 2308–2319 (2020)
12. K. Ali, S.A. Khan, M.Z. Mat-Jafri, Effect of double layer (SiO_2/TiO_2) anti-reflective coating on silicon solar cells. Int. J. Electrochem. Sci. **9**, 7865–7874 (2014)
13. L. Claudio Andreani, A. Bozzola, P. Kowalczewski, M. Liscidini, L. Redorici, Silicon solar cells: toward the efficiency limits. Adv. Phys. **4**(1), 1548305 (2019)
14. R. Cariou, J. Benick, F. Feldmann et al., III–V-on-silicon solar cells reaching 33% photoconversion efficiency in two-terminal configuration. Nat. Energy **3**, 326–333 (2018)
15. F. Schindler, A. Fell, R. Müller, J. Benick, A. Richter, F. Feldmann, P. Krenckel, S. Riepe, M.C. Schubert, S.W. Glunz, Towards the efficiency limits of multicrystalline silicon solar cells. Sol. Energy Mater. Sol. Cells **185**, 198–204 (2018)
16. D.B. Mahadik, R.V. Lakshmi, H.C. Barshilia, High performance single layer nano-porous antireflection coatings on glass by sol–gel process for solar energy applications. Solar Energy Mater. Sol. Cells **140**, 61–68 (2015)
17. A.T. Salih, A.A. Najim, M.A.H. Muhi, K.R. Gbashi, Single-material multilayer ZnS as anti-reflective coating for solar cell applications. Optics Communications **388**, 84–89 (2017)
18. M. Sayem-Mozumder, I.M. Abdel-Hamid, H. Pervez, R. Surkatti, Recent developments in multifunctional coatings for solar panel applications: a review. Sol. Energy Mater. Sol. Cells **189**, 75–102 (2019)
19. A. Samet-Sarki, N. Ekren, S. Saglam, A review of anti-reflection and self-cleaning coatings on photovoltaic panels. Sol. Energy **199**, 63–73 (2020)
20. S. Bashir-Khan, Z. Zhang, S. Long-Lee, Single component: bilayer TiO_2 as a durable antireflective coating. J. Alloy Compd. **834**, 155137 (2020)
21. S.H. Jeong, J.K. Kim, B.S. Kim, S.H. Shim, B.T. Lee, Characterization of SiO_2 and TiO_2 films prepared using rf magnetron sputtering and their application to antireflection coating. Vacuum **4**(76), 505–517 (2004)
22. S.B. Khan, H. Wu, Z. Xie, W. Wang, Z. Zhang, Al_2O_3 encapsulated teflon nanostructures with high thermal stability and efficient antireflective performance. ACS Appl. Mater. Interfaces **9**(41), 36327–36337 (2017)
23. J. Yun, T.S. Bae, J.D. Kwon, S. Lee, G.H. Lee, Antireflective silica nanoparticle array directly deposited on flexible polymer substrates by chemical vapor deposition. Nanoscale **22**(4), 7221–7230 (2012)
24. C. Deng, H. Ki, Pulsed laser deposition of refractive-index-graded broadband antireflection coatings for silicon solar cells. Sol. Energy Mater. Sol. Cells **147**, 37–45 (2016)
25. C. Tao, L. Zhang, Fabrication of multifunctional closed-surface SiO_2-TiO_2 antireflective thin films. Colloid. Surface. Physicochem. Eng. Aspect. **585**, 124045 (2020)
26. W. Zhang, J. Tu, W. Long, W. Lai, Y. Sheng, T. Guo, Preparation of SiO_2 antireflection coatings by sol-gel method. Energy Procedia **130**, 72–76 (2017)
27. S.B. Khan, H. Wu, J. Li, L. Chen, Z. Zhang, Bilayer SiO_2 nanorod arrays as omnidirectional and thermally stable Antireflective coating. Adv. Eng. Mater. **20**, 1700942 (2018)
28. C. Yin, M. Zhu, T. Zeng, J. Sun, R. Zhang, J. Zhao, L. Wang, J. Shao, Al_2O_3 anti-reflection coatings with graded-refractive index profile for laser applications. Opt. Mater. Express **11**(3), 885–883 (2021)
29. Q.Y. Zhang, X.Y. Huang, Recent progress in quantum cutting phosphors. Prog. Mater Sci. **55**, 353–427 (2010)
30. S.W. Baek, J.H. Shim, H.M. Seung, G.S. Lee, J.P. Hong, K.S. Lee, J.G. Park, Effect of core quantum-dot size on power-conversion efficiency for silicon solar-cells implementing energy-downshift using CdSe/ZnS core/shell quantum dots. Nanoscale **6**, 12524–12531 (2014)

31. V. Amendola, R. Pilot, M. Frasconi, O.M. Marago, M.A. Lati, Surface plasmon resonance in gold nanoparticles: a review. J. Phys. **29**, 203002 (2017)
32. V. Amendola, F. Stellacci, O.M. Bakr, A study of the surface plasmon resonance of silver nanoparticles by the discrete dipole approximation method: effect of shape, size, structure, and assembly. Plasmonics **5**, 85–97 (2010)
33. P. Liu, H. Wang, X. Li, M. Rui, H. Zeng, Localized surface plasmon resonance of Cu nanoparticles by laser ablation in liquid media. RSC Adv. **5**, 79738 (2015)
34. X. Liu, L. Jia, G. Fan, J. Gou, S.F. Liu, B. Yan, Au nanoparticle enhanced thin-film silicon solar cells. Sol. Energy Mater. Sol. Cells **147**, 225–234 (2016)
35. J.A. Martinez-Zamora, D. Berman-Mendoza, A. Ramos-Carrazco, A. Vera-Marquina, H.J. Higuera Valenzuela, F. Romo-García, R.C. Carrillo-Torres, Efficiency enhancement of polycrystalline silicon solar cells by a downshifting coating of silicon nanoparticles. *Optical Interference Coatings Conference (OIC)*, R. Sargent and A. Sytchkova, eds., Technical Digest Series (Optica Publishing Group, 2022) (2022)
36. R. Lopez-Delgado, H.J. Higuera-Valenzuela, A. Zazueta-Raynaud, A. Ramos-Carrazco, J.E. Pelayo, D. Berman-Mendoza, M.E. Álvarez-Ramos, A. Ayon, Solar cell efficiency improvement employing down-shifting silicon quantum dots. Microsyst. Technol. **24**(1), 495–502 (2018)
37. F.I. Chowdhury, K. Islam, S. Alkis, B. Ortac, M. Alevli, N. Dietz, A. Okyay, A. Nayfeh, Enhanced Light scattering with energy downshifting using 16 nm indium nitride nanoparticles for improved thin-film a-Si N-I-P solar cells. ECS Trans. **66**, 9 (2015)
38. D. Walker, L.E. Colyott, N.A. Larsen, S.W.S. McKeever, The wavelength dependence of light-induced fading of thermoluminescence from a-Al2O3:C. Radiat. Meas. **26**(5), 711–718 (1996)
39. M.L. Chithambo, C. Seneza, F.O. Ogundare, Kinetic analysis of high temperature secondary thermoluminescence glow peaks in a-Al_2O_3:C. Radiat. Meas. **66**, 21–30 (2014)
40. A.N. Yazici, S. Solak, Z. Öztürk, M. Topaksu, Z. Yegingil, The analysis of dosimetric thermoluminescent glow peak of a-Al_2O_3: C after different dose levels by ß-irradiation. J. Phys. D **36**(2), 181–191 (2003)
41. J.F. Moulder, W.F. Stickle, P.E. Sobol, K.D. Domben, Handbook of X Ray Photoelectron spectroscopy (1992). https://doi.org/10.1002/0470014229.ch22.
42. T. F. Scientific, "Oxygen|XPS Periodic Table|Thermo Fisher Scientific-MX," 2022. https://www.thermofisher.com/mx/es/home/materials-science/learningcenter/periodic-table/non-metal/oxygen.html(accessedMar.14,2022).
43. T. F. Scientific, "Aluminum|XPS Periodic Table|Thermo Fisher Scientific-MX," 2022. https://www.thermofisher.com/mx/es/home/materials-science/learningcenter/periodic-table/other-metal/aluminium.html(accessedMar.14,2022).
44. H. G. Tompkins and E. A. Irene, "Handbook of Ellipsometry", 2005, doi: https://doi.org/10.1515/arh-2005-0022.
45. "Spectroscopic ellipsometry and reflectometry: a user's guide", *Choice Rev. Online*, **37**(01), 37–0379 (1999)
46. Handbook of Thin Film Materials. United States: College of Engineering and Applied Science, University of Rochester, (1979)
47. R.L. Puurunen, Random deposition as a growth mode in atomic layer deposition. Chem. Vap. Depos. **10**(3), 159–170 (2004)
48. J.R. Van Ommen, A. Goulas, and R.L. Puurunen, Atomic Layer Deposition. In Kirk-Othmer Encyclopedia of Chemical Technology, (2023)

Publisher's Note Springer Nature remains neutral with regard to jurisdictional claims in published maps and institutional affiliations.